

1 **Off-fault Focal Mechanisms not Representative of Interseismic Fault Loading**  
2 **Suggest Deep Creep on the Northern San Jacinto Fault**

3 **M. L. Cooke<sup>1</sup> and J. L. Beyer<sup>1</sup>**

4 <sup>1</sup>Geosciences Department, University of Massachusetts – Amherst, USA

5 Corresponding author: Michele Cooke ([cooke@geo.umass.edu](mailto:cooke@geo.umass.edu))

6 **Key Points:**

- 7     • Crustal deformation models demonstrate the plausibility of deep creep along the  
8       northern San Jacinto fault to account for nearby enigmatic normal slip mechanisms
- 9     • Microseismicity that records off-fault deformation may record stresses that differ from  
10      interseismic loading of the primary fault surfaces
- 11    • Where faults exhibit creep at any crustal level, caution should be used in the inversion  
12      of nearby focal mechanisms for interseismic fault loading

13

## 14 **Abstract**

15 Within the San Bernardino basin, some focal mechanisms show normal slip that is inconsistent  
16 with the expected interseismic strike-slip loading of the region. The discrepancy may owe to deep  
17 (> 10 km depth), creep along the nearby northern San Jacinto fault. The enigmatic normal slip  
18 microseismicity occurs to the northeast of the fault and primarily below 10 km depth, consistent  
19 with off-fault deformation due to spatially non-uniform on-going slip. Consequently, if these  
20 normal focal mechanisms are included in stress inversions from the seismic catalog, the results  
21 may provide inaccurate information about fault loading. Here, we show that off-fault loading from  
22 models with deep interseismic creep on the northern San Jacinto fault match the first-order pattern  
23 of observed normal slip focal mechanisms in the basin and that this deep creep cannot be detected  
24 with GPS data due to the proximity of the San Andreas fault.

## 25 **Plain Language Summary**

26 Over the past 36 years, seismic stations have recorded the style of deformation from thousands of  
27 small earthquakes in the San Bernardino basin, California. Within this basin, many earthquakes  
28 below 10 km depth show deformation that doesn't match what we expect for this region during  
29 the current period between large damaging earthquakes along the San Jacinto and San Andreas  
30 faults. Rather than showing expected horizontal slip, many of these earthquakes show vertical  
31 movement. We use crustal deformation models to show that vertical movement can be produced  
32 in the basin if the northern portion of the San Jacinto fault creeps at depth; this portion of the  
33 fault is constantly moving rather than locked, like the San Andreas fault. Traditional GPS-based  
34 approaches to detect deep creep don't work here because the faults are too close to one another.  
35 The findings of this study demonstrate that small earthquakes that occur adjacent to and between  
36 faults can have very different style of deformation than the large ground rupturing earthquakes  
37 produced along active faults. This means that scientists should not use the information recorded  
38 by these small earthquakes in the San Bernardino basin to predict loading of the nearby San  
39 Andreas and San Jacinto faults.

## 40 **1 Introduction**

41 Earthquake rupture simulations that can inform regional seismic hazards are sensitive to  
42 estimates of current stress state along active faults (e.g., Harris et al., 2009; Ryan et al., 2015).  
43 Whereas borehole data from some localities can provide stress state information within the near  
44 surface, we rely exclusively on microseismicity data to inform the stress state throughout the  
45 seismogenic crust (e.g., Hardebeck & Hauksson, 2001; Heidbach et al., 2010). One assumption  
46 built into estimates of stress state from microseismicity is that the seismic catalog collected over  
47 the past several decades accurately represents the loading of active faults within California. This  
48 assumption is challenged by the limited duration of the seismic catalog compared to the 100-  
49 1000-year recurrence intervals along most faults within California. For example, in the  
50 earthquake catalog, the San Andreas fault (SAf) south of Cajon Pass has had fewer earthquakes  
51 than nearby faults (e.g. Yang et al., 2012). Although the San Andreas fault has the greatest  
52 potential for large earthquakes in southern California (e.g. Field et al., 2014), it is relatively  
53 under-sampled within the seismic catalog because the fault is locked between the times of large  
54 earthquakes. Furthermore, small earthquakes in the crust may record off-fault deformation rather  
55 than slip along the primary slip planes of active faults (Cheng et al., 2018). Where off fault  
56 deformation differs from loading of the primary faults, the stress state inferred from

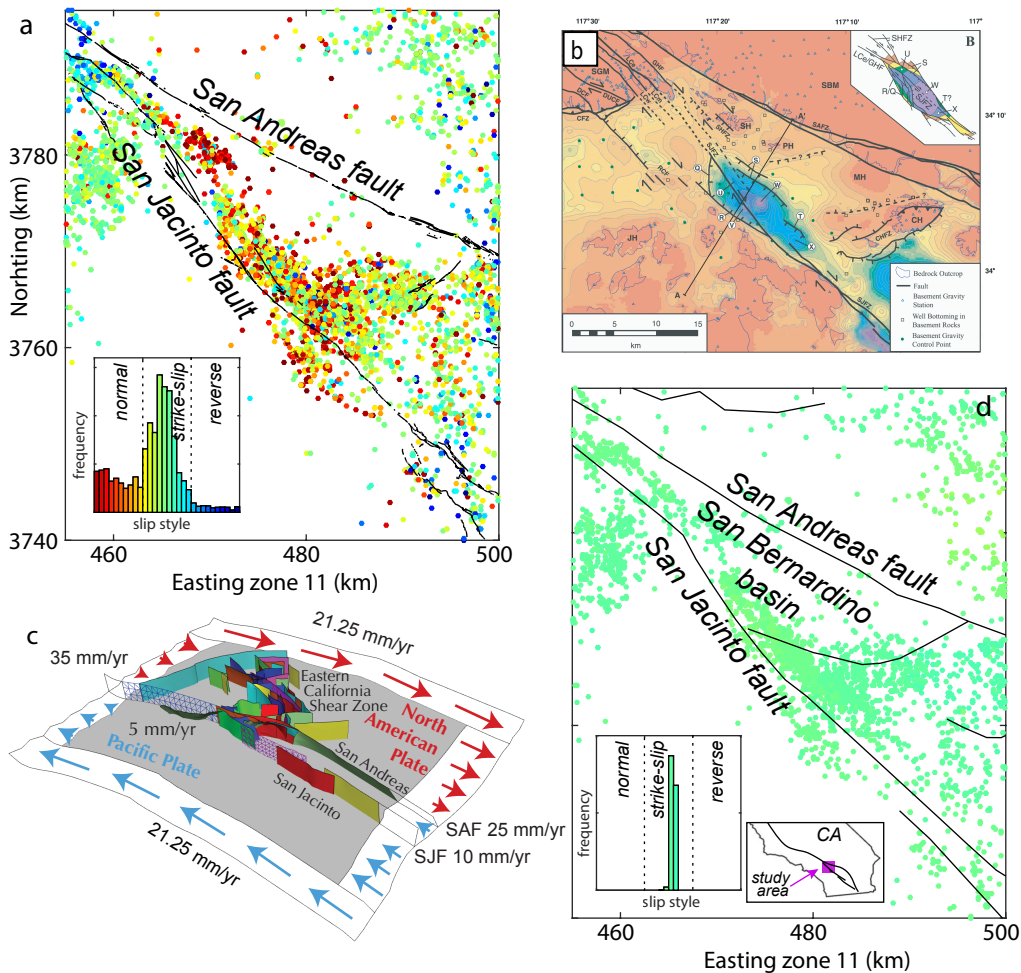


Figure 1. a) Focal mechanisms with nodal plane uncertainty  $< 45^\circ$  from 1981 through September of 2016 in the relocated catalog of (Yang et al., 2012 and subsequent updates available from SCEC) with surface traces of faults active within the last 15 ka (USGS & CGS, 2006). Colors show slip sense as  $\tan(\text{slip rake})$  scaled to the 0-3 range of  $A\phi$  slip sense (Simpson, 1997). b) Basement depth inverted from gravity data shows secondary normal faults that flank the San Jacinto fault (taken from Anderson et al., 2004). The normal slip focal mechanisms extend beyond the interpreted graben. c) Model of 63 active faults in the region used to build the steady state and interseismic models of crustal deformation. The lateral edges of the horizontal crack are loaded with plate velocities to simulate the regional tectonic loading (taken from Beyer et al., in press). d) Slip sense predicted by interseismic crustal deformation model of b) at locations of the earthquakes recorded in the catalog. Traces of modeled faults shown in black. Insets of a) and d) show histograms of slip sense. The normal slip focal mechanisms within the San Bernardino basin are not expected from interseismic loading of completely locked San Andreas and San Jacinto faults.

57 microseismicity may not accurately reflect the interseismic loading of the major active faults  
58 capable of producing ground rupturing earthquakes.

59         While we might expect the focal mechanisms from recorded microseismicity along the  
60 southern SAf system to reveal that dextral deformation dominates this system, Yang et al. (2013)  
61 show that some regions, such as the San Bernardino basin, produce predominantly normal-slip  
62 microseismicity (Fig. 1a). These focal mechanisms contrast the observations of long-term strike-  
63 slip along the nearby SAf (e.g., McGill et al., 2013, 2015) and San Jacinto fault (SJf) (e.g.,  
64 Anderson et al., 2004; Onderdonk et al., 2015). The normal slip focal mechanisms also disagree  
65 with crustal deformation models of the region that show dextral interseismic loading of the  
66 region (e.g., Johnson, 2013; Loveless & Meade, 2011; Smith-Konter et al., 2011). This  
67 discrepancy suggests that some of the recent microseismicity in the San Bernardino basin is not  
68 consistent with the expected loading of the SAf and SJf flanking the basin.

69         Slip gradients along strike-slip faults, such as near the tips of earthquake ruptures, can  
70 produce off-fault stresses and subsequent aftershocks that differ from the loading of the faults  
71 (e.g., Hardebeck, 2014; Oppenheimer, 1990). Yang et al. (2012) report temporary changes in  
72 focal mechanism slip sense after large magnitude earthquakes in southern California. Cheng et  
73 al. (2018) report off-fault aftershocks that have different slip sense from the earthquakes that  
74 occur along the Anza segment of the San Jacinto fault, to the south of the study area of this  
75 paper. Some of the normal slip earthquakes within the San Bernardino basin have been  
76 associated with secondary normal faults revealed by geophysical imaging of the top of the  
77 basement (Anderson et al., 2004). Small normal faults trend sub-parallel to the SJf and bound the  
78 edges of a local graben that developed where the SJf changes strike (Fig. 1b). While strike-slip  
79 along the San Jacinto and/or San Andreas faults could promote extension of this graben and  
80 normal slip microseismicity in the San Bernardino basin, all faults in the region are presumed to  
81 be locked during the interseismic period of the seismic catalog. Furthermore, the last large slip  
82 event in the region was over 200 years ago in 1812, (e.g., Lozos, 2016) and the current seismic  
83 catalog should be free of effects from that earthquake. The observation of normal slip  
84 microseismicity in the San Bernardino basin remains enigmatic in this region of dextral  
85 interseismic loading (Fig. 1d).

86         We propose that some degree of unlocking of the San Jacinto fault could account for the  
87 observation of recent normal slip earthquakes in the San Bernardino basin. Spatially non-  
88 uniform creep at depth along the northern SJf may produce some degree of local extension  
89 within the basin. Consequently, the microseismicity in our multi-decadal catalog may record  
90 both interseismic dextral loading of the region as well as off-fault deformation associated with  
91 deep creep on the northern SJf. We use crustal deformation models to show the potential for slip  
92 to produce off-fault microseismicity that obfuscates our interpretation of fault loading from the  
93 seismic catalog.

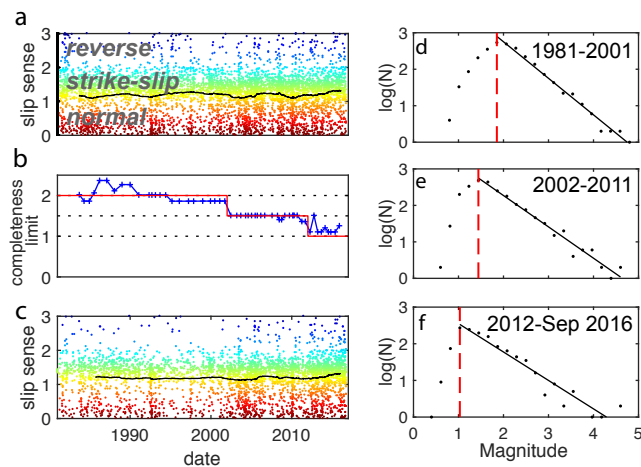


Figure 2. a) Focal mechanisms from Hauksson et al. (2012) within the region of Figure 1. The average slip sense for moving window of 600 earthquakes shown with black line. Warm colors are normal, cool colors are reverse, and green are strike-slip earthquakes. b) Magnitude completeness limit for a moving window of 600 earthquakes advanced in 100 earthquake increments shown in blue. The stepped red line shows the three estimated stages of magnitude completeness during the record. c) The 3920 focal mechanisms that exceed the three-phased magnitude completeness limit have mean  $A\phi$  of  $1.2 \pm 0.04$ , indicating limited variation in slip sense during the record. These earthquakes range in magnitude from 1 to 4.8 and depths from 1.2-20 km. (d-e) The log of frequency demonstrates the completeness of the catalog for each epoch: 1981 through 2001 (d), 2002 through 2011 (e) and after 2012 (f). The completeness limit (red dashed line) decreases in each successive epoch.

94 **2. Methods**

## 95 2.1 Reliable catalog of focal mechanisms in the San Bernardino basin

96 We analyze the three-dimensional distribution of focal mechanisms in the San  
97 Bernardino basin to assess the spatial pattern of the enigmatic normal slip microseismicity. A  
98 catalog of relocated southern California focal mechanisms from January 1981 through  
99 September 2016 are available from the Southern California Earthquake Center database  
100 (Hauksson et al., 2012; Yang et al., 2012). We limit the analysis to high-quality focal  
101 mechanisms described by Yang et al. (2012) to have nodal plane uncertainty  $< 45^\circ$ . Figure 2a  
102 shows the 6081 focal mechanisms between Easting 455000 and 500000 meters UTM zone 11  
103 and Northing 3740000 and 3795000 meters. In this region, the mean slip sense assessed with a  
104 600-earthquake moving window remains around  $A\phi = 1.2$  during the time period of the seismic  
105 catalog, indicating overall normal and strike-slip focal mechanisms (black line on Fig. 2a).

106 Excluding earthquakes smaller than the magnitude completeness limit eliminates bias of  
107 including small earthquakes that are recorded because they occur close to seismic instruments.  
108 The completeness limit of the San Bernardino basin subset of the seismic catalog improves with  
109 time as seismic stations are added to the network. We calculate the evolving magnitude  
110 completeness limit using the maximum curvature method (Wiemer & Wyss, 2000) for a moving  
111 window of 600 earthquakes advanced in increments of 100 earthquakes. The magnitude  
112 completeness improves around 2002 and 2012 so that we can define three epochs of magnitude  
113 completeness limits (red line on Fig. 2b). To determine a reliable focal mechanism catalog that  
114 exceed completeness, we exclude earthquakes smaller than M2 for epoch1 (1981 – 2001),  
115 smaller than M1.5 for epoch2 (2002-2011), and smaller than M1.0 for epoch3 (2012 –  
116 September 2016). The resulting catalog of 3920 reliable focal mechanisms shows consistent slip  
117 sense ( $A\phi = 1.2$ ) throughout the 36-year catalog, suggesting that the catalog is not significantly  
118 impacted by transient changes, such as stress changes from nearby large earthquakes or  
119 anomalous periods of enhanced normal faulting (Fig. 2c).

## 120 2.2 Steady-state and interseismic crustal models of the region

121 To simulate the stresses in the San Bernardino basin that drive interseismic  
122 microseismicity, we have developed 3D Boundary Element Method stressing rate models that  
123 simulate interseismic loading between earthquakes using a two-step approach. For the first step,  
124 multiple earthquake cycles are simulated in a steady-state model where all portions of the fault  
125 surfaces slip. The second step of the approach implements a back-slip approach to simulate the  
126 interseismic loading of the faults, where the slip distribution from the steady-state model is applied  
127 to faults below the prescribed locking depth (e.g., Marshall et al., 2009).

128 For the first stage of interseismic model development, we produce a steady-state model of  
129 crustal deformation over many earthquake cycles. The model incorporates active fault surfaces  
130 of the region based on the SCEC Community Fault Model v. 4.0 (Nicholson et al., 2013; Plesch  
131 et al., 2007) and re-meshed for more uniform triangular element size and coincident nodes along

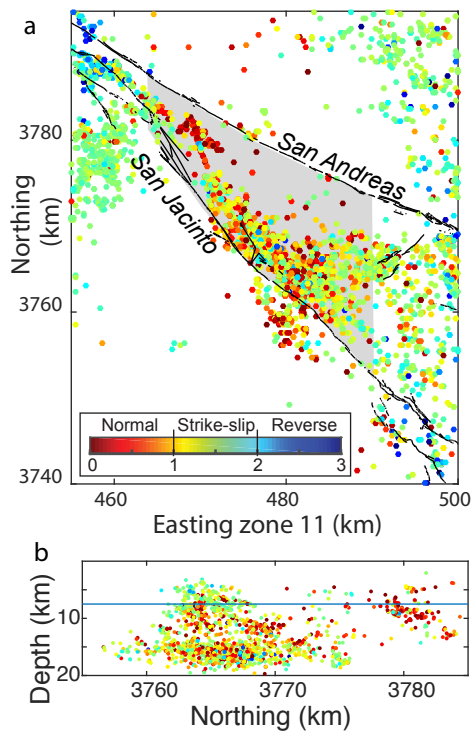


Figure 3. a) Map view of reliable focal mechanisms that pass the completeness test colored by slip sense. Normal focal mechanisms occur within the San Bernardino basin, between the San Andreas and San Jacinto faults. Dashed fault traces are the graben bounding normal faults imaged by Anderson (2004) in Fig. 1C. b) Focal mechanisms of the San Bernardino basin (grey region of a) projected into a N-S profile. Slip sense color same as in a. The normal slip focal mechanisms within the San Bernardino basin occur predominantly below 7.5 km depth

132 fault intersections (Fig. 1c). While based on version 4.0 of the CFM, the fault model includes  
133 revised fault surfaces in the Eastern California Shear Zone and elsewhere that give better match  
134 to geologic slip rates (e.g., Fattaruso et al., 2014; Justin W. Herbert et al., 2014) and honors the  
135 mapped active fault traces of the USGS fault and fold database (USGS & CGS, 2006). The fault  
136 geometry used in this study follows that of the preferred model of Beyer et al. (in press) with  
137 revised resolution of the San Jacinto fault (average element length  $\sim 2.6$  km). Within the 3D  
138 models, faults are extended to 35 km depth, where they merge with a horizontal crack.  
139 Deformation along this crack simulates distributed deformation below the seismogenic crust.  
140 Following Beyer et al. (in press), this study applies a plate tectonic movement equivalent to 47.5  
141 mm/yr at  $322.5^\circ$  (e.g., DeMets et al., 2010) to the sides of the model that parallel plate velocity  
142 and a velocity gradient along the sides of the model perpendicular to plate velocity. Where faults  
143 meet the lateral edges of the model, the applied velocity has a step and corresponding slip rates  
144 are applied to the endmost patch of the fault to avoid slip rates going to zero at these artificial  
145 fault tips (Fig. 1c). The shear traction-free faults in the center of the model slip in response to  
146 tectonic loading and interaction with each other. This low shear traction simulates dynamic  
147 conditions when most of the fault slip occurs.

148 To simulate interseismic loading between large earthquakes, the interseismic models  
149 apply slip rates from the long-term model below a prescribed locking depth. Using this  
150 approach, these interseismic models can simulate deep creep. To avoid a sharp step between  
151 slipping and locked regions, fault elements within a 2.5 km high transitional band above the  
152 locking depth are prescribed 50% of the slip rate values of the long-term model. We explore the  
153 impact of varying locking depth from 7.5 to 20 km along the San Jacinto fault while all other  
154 faults have a 20 km locking depth. In all the models, stress tensors are sampled at points in the  
155 model corresponding to the three-dimensional locations of reliable focal mechanisms. This  
156 allows the model results to be directly compared to the observed seismicity.

### 157 **3. Focal mechanism distribution supports deep creep along the northern San Jacinto fault**

158 Three aspects of the three-dimensional distribution of interseismic microseismicity in the  
159 San Bernardino basin are consistent with some degree of deep on-going interseismic slip along  
160 the northern SJf. Firstly, the contrast of high rate of microseismicity along the SJf compared to  
161 the quiet nearby SAF (Fig. 3a). Observations of abundant microseismicity adjacent to creeping  
162 faults (e.g., Harris, 2017) support the inference that the SJf could have active creep whereas the  
163 SAF is currently locked. Secondly, projecting the focal mechanisms of the reliable catalog into a  
164 north-south profile reveals that most of the normal slip focal mechanisms of the San Bernardino  
165 basin occur below  $\sim 7.5$  km depth (Fig. 3b). If the on-going SJf slip is contributing to the off-fault  
166 normal slip microseismicity, then the fault below this depth may be creeping. Along the Anza  
167 section of the San Jacinto fault, south of this study area, normal slip microseismicity also occurs  
168 near the SJf at depths of 10-13 km (Cheng et al., 2018). The discrepancy between locking depth  
169 of the Anza section of the SJf and base of seismicity have led to the inference of creep below 10



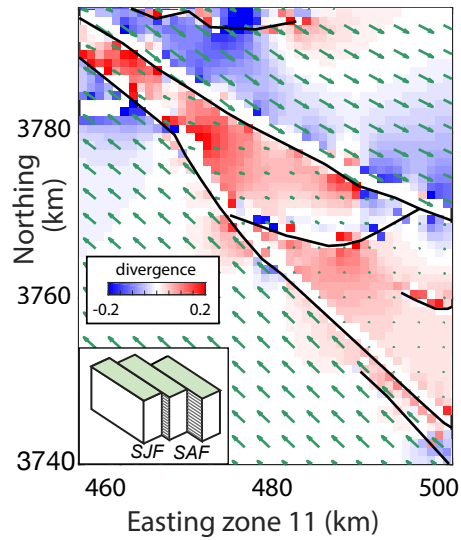


**Figure 4.** Green arrows show the velocities from the steady state model that simulates many earthquake cycles. The divergence of this velocity field reveals regions of overall contraction (negative dilation blue) and extension (positive dilation red) due to slip distribution along the faults. Inset cartoon shows the set-up of the steady-state model.

170 km along this section of the SJf (Wdowinski, 2009), consistent with the depths of off-fault  
171 normal microseismicity.

172         The third aspect of the focal mechanism distribution that supports deep on-going  
173 interseismic slip is that the normal slip focal mechanisms are primarily located northeast, and not  
174 southwest, of the SJf (Fig. 3a). Regional extension should produce normal slip microseismicity  
175 on both sides of interseismic locked faults. However, this pattern is consistent with the results of  
176 steady-state crustal deformation models of the region that simulate deformation over multiple  
177 earthquake cycles (Resor et al., 2018; Fig. 4b). This model shows a southward increasing dextral  
178 slip rate along the northern San Jacinto fault that produces a region of positive dilation (increased  
179 mean normal tension) within the San Bernardino basin. This long-term dilation can promote  
180 normal slip microseismicity at distances far from the fault by unclamping potential slip surfaces  
181 relative to those outside of the basin. The location of off-fault dilation correlates to the location  
182 of slip rate gradient along the SJf (Fig. 4b). Consequently, deep dilation consistent with the  
183 occurrence of normal slip microseismicity below  $\sim 7.5$  km in the San Bernardino basin may be  
184 associated with on-going slip along the SJf below  $\sim 7.5$  km. Deep on-going slip on the San  
185 Andreas fault could also produce dilation in the San Bernardino basin but the lack of  
186 microseismicity along the SAF suggests that this fault is locked. Taken together, the three-  
187 dimensional distribution of focal mechanisms within the San Bernardino basin is consistent with  
188 southward increasing creep rate along the northern SJf at depth.

#### 189 **4. Simulating deep creep on the northern San Jacinto fault**

190         To investigate the impact of deep interseismic creep on the northern San Jacinto fault, we  
191 investigate the sensitivity of focal mechanism slip sense within the San Bernardino basin to  
192 locking depth along the northern SJf (San Bernardino and San Jacinto Valley segments). The  
193 interseismic models apply 20 km locking depth on all other faults, consistent with the general  
194 base of seismicity of the region (e.g. Yang et al., 2012). The overall slip sense of  
195 microseismicity within the San Bernardino basin (grey region in Fig. 5a) is best matched by  
196 interseismic models with locking depth  $< 12.5$  km along the northern SJf (Fig. 5b). Results for  
197 locking depths of 7.5 and 10 km show similar fit within  $1\sigma$ . The interseismic model with 10 km  
198 locking depth produces normal slip that is spatially consistent with the observed enigmatic  
199 normal slip focal mechanisms within the San Bernardino basin (Fig. 5a). The normal slip in the  
200 interseismic model occurs to the northeast of the San Jacinto fault near the gradient in dextral  
201 slip rate along the fault.

202         While creep below 10-13 km has been inferred along the southern San Jacinto fault from  
203 geodetic evidence of shallow locking depths (Fialko, 2006; Smith-Konter et al., 2011;  
204 Wdowinski, 2009), geodetic inversions for the northern San Jacinto fault suggest a deep ( $\sim 20$   
205 km) locking depth (Smith-Konter et al., 2011). Because the San Jacinto and San Andreas faults  
206 approach within 10 km of each other at the San Bernardino basin, the inversions of geodetic data  
207 for locking depth in this region may not distinguish the independent locking depths of the SJf  
208 and SAF. To explore this, we compare the interseismic velocities at GPS sites from two models:

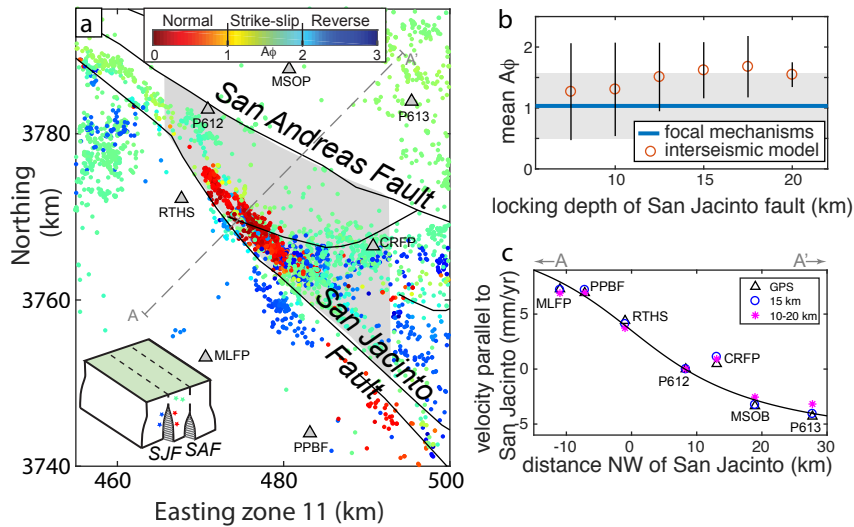


**Figure 5.** a) Slip sense at locations of microseismicity from the interseismic model with shallow locking depth (10 km) on the San Jacinto fault to simulate deep creep. The locking depth on other faults is 20 km. Inset cartoon shows the set-up of the interseismic model. Normal loading occurs at focal mechanism sites within the San Bernardino basin. GPS stations shown with labeled triangles. b) Mean interseismic loading within light grey region of A shown with  $1\sigma$  vertical bars. Models with SJf locking depth  $< 12.5$  km better match the mean slip sense of focal mechanisms in the San Bernardino Basin. c) Transect along A-A' (shown in A) of GPS station velocity parallel to the San Jacinto fault (Herbert et al., 2014), and velocity predictions from the interseismic model with a shallow locking depth on the SJf (pink star, same as results shown in a) and interseismic model with a 15 km locking depth on all faults (blue circle). The surface velocities cannot resolve deep slip on the SJf because of its proximity to the SAF.

209 one that has 15 km locking depth on all faults and another that has 10 km locking depth on the  
210 northern SJf and 20 km on all other faults. The station velocities from the two models cannot be  
211 distinguished from the observed GPS station velocities determined by Herbert et al. (2014) (Fig.  
212 5c). Consequently, geodetic data cannot eliminate deep creep on the northern San Jacinto fault as  
213 a potential mechanism for the off-fault normal slip microseismicity within the San Bernardino  
214 basin.

## 215 5. Discussion

216 Both the observed focal mechanisms and the model predicted slip show both normal and strike-  
217 slip microseismicity in the San Bernardino basin. Some differences in the predicted interseismic  
218 slip sense at locations of microseismicity and observed slip sense reveal aspects of the model that  
219 may not adequately capture the 3D complexity of active deformation along the San Jacinto fault.  
220 Within the model, normal slip microseismicity occurs within a narrow band adjacent to the SJf  
221 with strike- and reverse slip outside of this band where the catalog records a combination of  
222 normal and strike-slip focal mechanisms. The model may over-predict the proportion of normal  
223 focal mechanisms for several potential reasons. Firstly, the model calculates the slip sense on  
224 the most preferentially oriented slip plane off of the fault but, if instead, the microseismicity  
225 occurs on preexisting structures, the observed slip sense may differ from the model prediction.  
226 Similarly, the model does not consider interaction between earthquakes such as local normal  
227 microseismicity after small strike-slip earthquakes (Cheng et al., 2018). Another consideration is  
228 that the model may over-predict normal slip because the model incorporates complete unlocking  
229 of the SJf below the locking depth whereas partial unlocking may provide an off-fault stress state  
230 between that of dilation and interseismic strike-slip loading of the region.

231 Within the model, faults that may have damage zones and complex secondary structures  
232 are modeled as single slip surfaces discretized into elements with constant slip. The nature of  
233 fault surface discretization within the model leads to artificially linear and abrupt transitions  
234 from slipping to transitional ( $1/2$  long term slip rate) to locked portions of the fault. These abrupt  
235 transitions may produce a more localized pattern of normal slip microseismicity than observed.  
236 Furthermore, the model does not consider host rock heterogeneities and deformation along  
237 secondary faults (e.g. Anderson et al., 2004) that could act to promote interseismic normal slip  
238 microseismicity over a wider region. For example, deep creep along strands parallel to the  
239 modeled San Jacinto fault would broaden the predicted zone of off-fault normal faulting. Our  
240 analysis does not distinguish between localized creep on a single plane and a narrow zone of  
241 distributed creep, and either of these scenarios may be occurring at depth along the SJf.

242 A rich aftershock catalog from the recent Borrego Springs 2016 earthquake shows  
243 evidence for a distributed zone of on-going deformation along southern San Jacinto fault where it  
244 splits into three sub-parallel strands (Ross et al., 2017). A similar investigation for the northern  
245 San Jacinto fault may yield further insight into the detailed structure of the fault. For example,  
246 such a study might confirm secondary structures that were interpreted from early seismic  
247 catalogs by Nicholson et al. (1986).

248 Deep creep along the northern San Jacinto fault may impact seismic hazard estimates on  
249 this fault. Both the accommodation of slip along the fault and the accommodation of off-fault

250 deformation within the adjacent crust via microseismicity and aseismic pervasive deformation  
251 mechanisms may reduce the interseismic loading on the deeper portion of the northern SJf,  
252 thereby reducing seismic hazard. We might also expect moderate or large earthquakes to  
253 nucleate at the transition between creeping and locked portions (Harris, 2017). Shallow sections  
254 of the northern SJf may have increased loading due to deep creep and greater potential for large  
255 earthquakes.

256 The correlation between the slip sense of focal mechanisms in the San Bernardino basin  
257 and patterns of off-fault stressing rate from interseismic models with ~10 km locking depth on  
258 the San Jacinto fault suggests that the interseismic microseismicity of the basin records a  
259 component of permanent distributed off-fault deformation in the basin. This result is consistent  
260 with a recent study of normal slip focal mechanisms along the Anza section of the SJf (Cheng et  
261 al., 2018). If the focal mechanisms of the basin were inverted to estimate interseismic stresses on  
262 the SJf and SAF, they would predict normal loading contrary to the long-term slip record of these  
263 faults. Using microseismicity that records this off-fault deformation may produce erroneous  
264 estimates of interseismic fault loading. Within the San Bernardino basin, the errors of focal  
265 mechanism inversions for fault stressing rate are compounded by the under-sampling of strike-  
266 slip earthquakes along the relatively quiet SAF. This study suggests that where faults creep,  
267 spatially non-uniform creep rates may produce heterogeneous off-fault deformation. Geodesy  
268 around the juncture of the creeping section of the San Andreas fault with the locked Carrizo  
269 section show off-fault dilation due to similar spatial gradient in creep rate as proposed here  
270 (Titus et al., 2011). Where faults exhibit creep at any crustal level, caution should be used when  
271 incorporating off-fault focal mechanisms to infer interseismic fault loading.

272

### 273 **Acknowledgments, Samples, and Data**

274 This research was supported by the Southern California Earthquake Center (Contribution No.  
275 8079). SCEC is funded by NSF Cooperative Agreement EAR-1033462 & USGS Cooperative  
276 Agreement G12AC20038. Reviews by Ruth Harris and Zachary Ross greatly improved this  
277 manuscript. The authors thank Scott Marshall for sharing his Poly3D executable code and many  
278 insightful discussions. Model results of slip sense sampled at locations of microseismicity for the  
279 interseismic models with various locking depth are available on figshare (Cooke, 2018).

280

### 281 **References**

- 282 Anderson, M., Matti, J., & Jachens, R. (2004). Structural model of the San Bernardino basin,  
283 California, from analysis of gravity, aeromagnetic, and seismicity data. *Journal of*  
284 *Geophysical Research: Solid Earth*, 109(4). <https://doi.org/10.1029/2003JB002544>
- 285 Beyer, J. L., Cooke, M. L., & Marshall, S. T. (2018). Sensitivity of deformation to activity along  
286 the Mill Creek and Mission Creek strands of the San Andreas fault. *Geosphere Special*  
287 *Issue on Seismotectonics of the San Geronio Pass Region*.
- 288 Cheng, Y., Ross, Z. E., & Ben-Zion, Y. (2018). Diverse Volumetric Faulting Patterns in the San  
289 Jacinto Fault Zone. *Journal of Geophysical Research: Solid Earth*, 123(6), 5068–5081.

- 290 <https://doi.org/10.1029/2017JB015408>
- 291 Cooke, M. (2018). *Modeled slip style at locations of microseismicity within the San Bernardino*  
 292 *basin, CA*. <https://doi.org/10.6084/m9.figshare.6361022.v2>
- 293 Craig, N., Leonardo, S., Patrick, W., & R., S. L. (1986). Seismic evidence for conjugate slip and  
 294 block rotation within the San Andreas Fault System, southern California. *Tectonics*, 5(4),  
 295 629–648. <https://doi.org/10.1029/TC005i004p00629>
- 296 DeMets, C., Gordon, R. G., & Argus, D. F. (2010). Geologically current plate motions.  
 297 *Geophysical Journal International*, 181(1), 1–80. [https://doi.org/10.1111/j.1365-](https://doi.org/10.1111/j.1365-246X.2009.04491.x)  
 298 [246X.2009.04491.x](https://doi.org/10.1111/j.1365-246X.2009.04491.x)
- 299 Fattaruso, L. A., Cooke, M. L., & Dorsey, R. J. (2014). Sensitivity of uplift patterns to dip of the  
 300 San Andreas fault in the Coachella Valley, California. *Geosphere*, 10(6).  
 301 <https://doi.org/10.1130/GES01050.1>
- 302 Fialko, Y. (2006). Interseismic strain accumulation and the earthquake potential on the southern  
 303 San Andreas fault system. *Nature*, 441(7096), 968–971.  
 304 <https://doi.org/10.1038/nature04797>
- 305 Hardebeck, J. L. (2014). The impact of static stress change, dynamic stress change, and the  
 306 background stress on aftershock focal mechanisms. *Journal of Geophysical Research: Solid*  
 307 *Earth*, 119(11), 8239–8266.
- 308 Hardebeck, J. L., & Hauksson, E. (2001). Crustal stress field in southern California and its  
 309 implications for fault mechanics. *Journal of Geophysical Research: Solid Earth*, 106(B10),  
 310 21859–21882. <https://doi.org/10.1029/2001JB000292>
- 311 Harris, R. A. (2017). Large earthquakes and creeping faults. *Reviews of Geophysics*, 55(1), 169–  
 312 198. <https://doi.org/10.1002/2016RG000539>
- 313 Harris, R. A., Barall, M., Archuleta, R., E. Dunham, E., Aagaard, B., Ampuero, J. P., et al.  
 314 (2009). The SCEC/USGS Dynamic Earthquake Rupture Code Verification Exercise.  
 315 *Seismological Research Letters*, 80(1), 119–126. Retrieved from  
 316 <http://dx.doi.org/10.1785/gssrl.80.1.119>
- 317 Hauksson, E., Yang, W., & Shearer, P. M. (2012). Waveform relocated earthquake catalog for  
 318 Southern California (1981 to June 2011). *Bulletin of the Seismological Society of America*,  
 319 102(5), 2239–2244. <https://doi.org/10.1785/0120120010>
- 320 Heidbach, O., Tingay, M., Barth, A., Reinecker, J., Kurfeß, D., & Müller, B. (2010). Global  
 321 crustal stress pattern based on the World Stress Map database release 2008. *Tectonophysics*,  
 322 482(1), 3–15. <https://doi.org/https://doi.org/10.1016/j.tecto.2009.07.023>
- 323 Herbert, J. W., Cooke, M. L., Oskin, M., & Difo, O. (2014). How much can off-fault  
 324 deformation contribute to the slip rate discrepancy within the eastern California shear zone?  
 325 *Geology*, 42(1), 71–75. <https://doi.org/10.1130/G34738.1>
- 326 Herbert, J. W., Cooke, M. L., & Marshall, S. T. (2014). Influence of fault connectivity on slip  
 327 rates in southern California: Potential impact on discrepancies between geodetic derived  
 328 and geologic slip rates. *Journal of Geophysical Research: Solid Earth*, 119(3).  
 329 <https://doi.org/10.1002/2013JB010472>

- 330 Johnson, K. M. (2013). Slip rates and off-fault deformation in Southern California inferred from  
331 GPS data and models. *Journal of Geophysical Research: Solid Earth*, 118(10), 5643–5664.  
332 <https://doi.org/10.1002/jgrb.50365>
- 333 Loveless, J. P., & Meade, B. J. (2011). Stress modulation on the San Andreas fault by  
334 interseismic fault: System interactions. *Geology*, 39(11), 1035–1038.  
335 <https://doi.org/10.1130/G32215.1>
- 336 Lozos, J. C. (2016). A case for historic joint rupture of the San Andreas and San Jacinto faults.  
337 *Science Advances*, 2(3), 1–8. <https://doi.org/10.1126/sciadv.1500621>
- 338 Marshall, S. T., Cooke, M. L., & Owen, S. E. (2009). Interseismic deformation associated with  
339 three-dimensional faults in the greater Los Angeles region, California. *Journal of*  
340 *Geophysical Research: Solid Earth*, 114(12). <https://doi.org/10.1029/2009JB006439>
- 341 McGill, S. F., Owen, L. A., Weldon, R. J., & Kendrick, K. J. (2013). Latest pleistocene and  
342 holocene slip rate for the San Bernardino Strand of the San Andreas Fault, Plunge Creek,  
343 Southern California: Implications for strain partitioning within the Southern San Andreas  
344 Fault system for the last ~35 k.y. *Bulletin of the Geological Society of America*, 125(1–2),  
345 48–72. <https://doi.org/10.1130/B30647.1>
- 346 McGill, S. F., Spinler, J. C., McGill, J. D., Bennett, R. A., Floyd, M. A., Fryxell, J. E., &  
347 Funning, G. J. (2015). Kinematic modeling of fault slip rates using new geodetic velocities  
348 from a transect across the Pacific-North America plate boundary through the San  
349 Bernardino Mountains, California. *Journal of Geophysical Research: Solid Earth*, 120(4),  
350 2772–2793. <https://doi.org/10.1002/2014JB011459>
- 351 Nicholson, C., Plesch, A., Sorlien, C., Shaw, J., & Hauksson, E. (2013). Updating the 3D fault  
352 set for the Community Fault Model (CFM-v4) and revising its associated fault database. In  
353 *Southern California Earthquake Center annual meeting*.
- 354 Onderdonk, N. W., McGill, S. F., & Rockwell, T. K. (2015). Short-term variations in slip rate  
355 and size of prehistoric earthquakes during the past 2000 years on the northern San Jacinto  
356 fault zone, a major plate-boundary structure in southern California. *Lithosphere*, 7(3), 211–  
357 234. <https://doi.org/10.1130/L393.1>
- 358 Oppenheimer, D. H. (1990). Aftershock slip behavior of the 1989 Loma Prieta, California  
359 earthquake. *Geophysical Research Letters*, 17(8), 1199–1202.
- 360 Plesch, A., Shaw, J. H., Benson, C., Bryant, W. A., Carena, S., Cooke, M., et al. (2007).  
361 Community Fault Model (CFM) for southern California. *Bulletin of the Seismological*  
362 *Society of America*, 97(6). <https://doi.org/10.1785/0120050211>
- 363 Resor, P. G., Cooke, M. L., Marshall, S. T., & Madden, E. H. (2018). Influence of Fault  
364 Geometry on the Spatial Distribution of Long-Term Slip with Implications for Determining  
365 Representative Fault-Slip Rates. *Bulletin of the Seismological Society of America*, XX(Xx).  
366 <https://doi.org/10.1785/0120170332>
- 367 Ross, Z. E., Hauksson, E., & Ben-Zion, Y. (2017). Abundant off-fault seismicity and orthogonal  
368 structures in the San Jacinto fault zone. *Science Advances*, 3(3).  
369 <https://doi.org/10.1126/sciadv.1601946>
- 370 Ryan, K. J., Geist, E. L., Barall, M., & Oglesby, D. D. (2015). Dynamic models of an earthquake

- 371 and tsunami offshore Ventura, California. *Geophysical Research Letters*, 42(16), 6599–  
372 6606. <https://doi.org/10.1002/2015GL064507>
- 373 Simpson, R. W. (1997). Quantifying Anderson's fault types. *Journal of Geophysical Research:*  
374 *Solid Earth*, 102(B8), 17909–17919. <https://doi.org/10.1029/97JB01274>
- 375 Smith-Konter, B. R., Sandwell, D. T., & Shearer, P. (2011). Locking depths estimated from  
376 geodesy and seismology along the San Andreas Fault System: Implications for seismic  
377 moment release. *Journal of Geophysical Research: Solid Earth*, 116(6), 1–12.  
378 <https://doi.org/10.1029/2010JB008117>
- 379 Survey, U. S. G., & Survey, C. G. (2006). Quaternary fault and fold database for the United  
380 States. Retrieved July 20, 2001, from <http://earthquake.usgs.gov/hazards/qfaults/>
- 381 Titus, S. J., Dyson, M., DeMets, C., Tikoff, B., Rolandone, F., & Bürgmann, R. (2011). Geologic  
382 versus geodetic deformation adjacent to the San Andreas fault, central California. *Bulletin*  
383 *of the Geological Society of America*, 123(5), 794–820. <https://doi.org/10.1130/B30150.1>
- 384 Wdowinski, S. (2009). Deep creep as a cause for the excess seismicity along the San Jacinto  
385 fault. *Nature Geoscience*, 2(12), 882–885. <https://doi.org/10.1038/ngeo684>
- 386 Wiemer, S., & Wyss, M. (2000). Minimum magnitude of completeness in earthquake catalogs:  
387 Examples from Alaska, the Western United States, and Japan. *Bulletin of the Seismological*  
388 *Society of America*, 90(4), 859–869. <https://doi.org/10.1785/0119990114>
- 389 Yang, W., & Hauksson, E. (2013). The tectonic crustal stress field and style of faulting along the  
390 Pacific North America plate boundary in southern California. *Geophysical Journal*  
391 *International*, 194(1), 100–117. <https://doi.org/10.1093/gji/ggt113>
- 392 Yang, W., Hauksson, E., & Shearer, P. M. (2012). Computing a large refined catalog of focal  
393 mechanisms for southern California (1981–2010): Temporal stability of the style of faulting.  
394 *Bulletin of the Seismological Society of America*, 102(3), 1179–1194.  
395 <https://doi.org/10.1785/0120110311>

396

397

398 **Figure Captions**

399 **Figure 1.** a) Focal mechanisms with nodal plane uncertainty  $< 45^\circ$  from 1981 through  
400 September of 2016 in the relocated catalog of (Yang et al., 2012 and subsequent updates  
401 available from SCEC) with surface traces of faults active within the last 15 ka (USGS & CGS,  
402 2006). Colors show slip sense as  $\tan(\text{slip rake})$  scaled to the 0–3 range of  $A\phi$  slip sense (Simpson,  
403 1997). b) Basement depth inverted from gravity data shows secondary normal faults that flank  
404 the San Jacinto fault (taken from Anderson et al., 2004). The normal slip focal mechanisms  
405 extend beyond the interpreted graben. c) Model of 63 active faults in the region used to build the  
406 steady state and interseismic models of crustal deformation. The lateral edges of the horizontal  
407 crack are loaded with plate velocities to simulate the regional tectonic loading (taken from Beyer  
408 et al., in press). d) Slip sense predicted by interseismic crustal deformation model of b at  
409 locations of the earthquakes recorded in the catalog. Traces of modeled faults shown in black.  
410 Insets of a) and d) show histograms of slip sense. The normal slip focal mechanisms within the



411 San Bernardino basin are not expected from interseismic loading of completely locked San  
412 Andreas and San Jacinto faults.

413

414 **Figure 2.** a) Focal mechanisms within the region of Figure 1. The average slip sense for a  
415 moving window of 600 earthquakes shown with black line. Warm colors are normal, cool colors  
416 are reverse, and green are strike-slip earthquakes b) Magnitude completeness limit for a moving  
417 window of 600 earthquakes advanced in 100 earthquake increments shown in blue. The stepped  
418 red line shows the three estimated stages of magnitude completeness during the record. C) The  
419 3920 focal mechanisms that exceed the three-phased magnitude completeness limit have mean  
420  $A\phi$  of  $1.2 \pm 0.04$ , indicating limited variation in slip sense during the record. These earthquakes  
421 range in magnitude from 1 to 4.8 and depths from 1.2-20 km. (d-e) The log of frequency  
422 demonstrates the completeness of the catalog for each epoch: 1981 through 2001 (d), 2002  
423 through 2011 (e) and after 2012 (f). The completeness limit (red dashed line) decreases in each  
424 successive epoch.

425

426 **Figure 3.** a) Map view of reliable focal mechanisms that pass the completeness test, colored by  
427 slip sense. Normal slip focal mechanisms occur within the San Bernardino basin, between the  
428 San Andreas and San Jacinto faults. Dashed fault traces are the graben bounding normal faults  
429 imaged by Anderson (2004) in Fig. 1c. b) Focal mechanisms of the San Bernardino basin (grey  
430 region of a) projected into a N-S profile. Slip sense color same as in a. The normal slip focal  
431 mechanisms within the San Bernardino basin occur predominantly below 7.5 km depth.

432

433 **Figure 4.** Green arrows show the velocities from the steady state model that simulates many  
434 earthquake cycles. The divergence of this velocity field reveals regions of overall contraction  
435 (negative dilation blue) and extension (positive dilation red) due to slip distribution along the  
436 faults. Inset cartoon shows the set-up of the steady-state model.

437

438 **Figure 5:** a) Slip sense at locations of microseismicity from the interseismic model with shallow  
439 locking depth (10 km) on the San Jacinto fault to simulate deep creep. The locking depth on all  
440 other faults is 20 km. Inset cartoon shows the set-up of the interseismic model. Normal loading  
441 occurs at focal mechanism sites within the San Bernardino basin. GPS stations shown with  
442 labeled triangles. b) Mean interseismic loading within light grey region of A shown with  
443  $1\sigma$  vertical bars. Models with SJf locking depth  $< 12.5$  km better match the mean slip sense of  
444 focal mechanisms in the San Bernardino Basin. c) Transect along A-A' (shown in A) of GPS  
445 station velocity parallel to the San Jacinto fault (J.W. Herbert et al., 2014), and velocity  
446 predictions from the interseismic model with a shallow locking depth on the SJf (pink star, same  
447 as results shown in A) and interseismic model with a 15 km locking depth on all faults (blue  
448 circle). The surface velocities cannot resolve deep slip on the SJf because of its proximity to the  
449 SAF.